Journal Pre-Proof

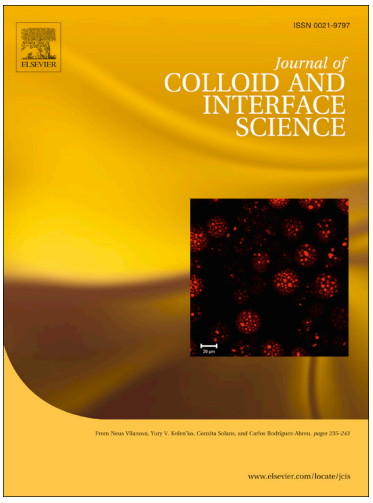

Comparison of hydrophobicity and durability of functionalized aluminium oxide nanoparticle coatings with magnetite nanoparticles - links between morphology and wettability

Donald Hill, Andrew R. Barron, Shirin Alexander

PII: S0021-9797(19)30860-4
DOI: https://doi.org/10.1016/j.jcis.2019.07.080
Reference: YJCIS 25225

To appear in: *Journal of Colloid and Interface Science*

Received Date: 13 June 2019
Revised Date: 25 July 2019
Accepted Date: 27 July 2019

Please cite this article as: D. Hill, A.R. Barron, S. Alexander, Comparison of hydrophobicity and durability of functionalized aluminium oxide nanoparticle coatings with magnetite nanoparticles - links between morphology and wettability, *Journal of Colloid and Interface Science* (2019), doi: https://doi.org/10.1016/j.jcis.2019.07.080

Comparison of hydrophobicity and durability of functionalized aluminium oxide nanoparticle coatings with magnetite nanoparticles - links between morphology and wettability

Donald Hill[a], Andrew R. Barron,[a,b,c] and Shirin Alexander[a,*]

[a] *Energy Safety Research Institute (ESRI), Swansea University Bay Campus, Fabian Way, Swansea SA1 8EN, United Kingdom.*

[b] *Department of Chemistry, Rice University, Houston, Texas 77005, United States.*

[c] *Department of Materials Science and Nanoengineering, Rice University, Houston, Texas 77005, United States.*

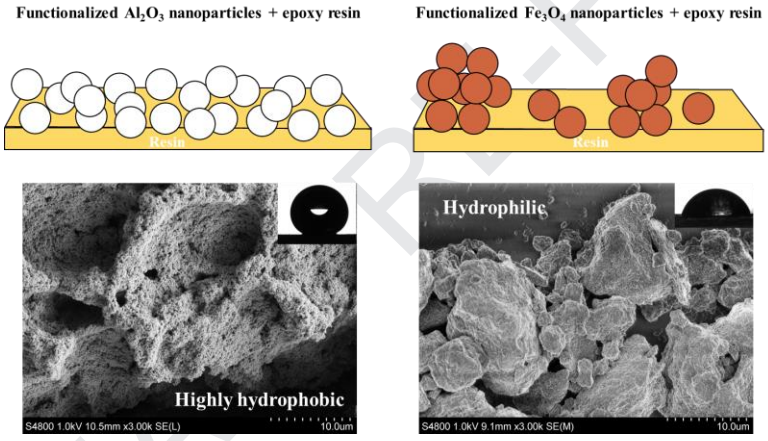

Abstract

Hypothesis

The wetting characteristics of coatings created using functionalised nanoparticles and adhesive resins, depends strongly on the particle distribution within the surface layers. Although it has been shown that commercially available adhesives improve the durability of hydrophobic nanoparticle coatings, the wettability of these surfaces is governed by the agglomeration behaviour of the particles within the adhesive. As a consequence of this, coatings where the particles are highly agglomerated within the adhesive show lower hydrophobicity.

Experiments

The morphology and chemical composition of coatings formed from carboxylate functionalised Al_2O_3 and magnetite (Fe_3O_4) nanoparticles and epoxy resin on plastic was

studied using scanning electron microscopy (SEM) and X-ray photoelectron spectroscopy (XPS). Water contact angle (WCA) measurements were used to investigate how the coatings' morphological characteristics and loading of the particles within the surface layers influenced their wettability. Infrared (IR) spectroscopy and thermogravimetric analysis (TGA) were used to study carboxylate adsorption onto the magnetite nanoparticles.

Findings

Combining the Al_2O_3 nanoparticles with epoxy resin was observed to create highly hydrophobic coatings that displayed water contact angles (WCAs) between 145-150°. These coatings displayed good durability when sonicated in isopropanol and wiped with tissue. By comparison, coatings formed from the magnetite nanoparticles were substantially less hydrophobic and displayed WCAs between 75-125° when combined with epoxy resin. SEM revealed that the magnetite nanoparticles in the coatings were present as large agglomerates. By comparison, coatings formed from the Al_2O_3 nanoparticles showed a more homogenous particle distribution. Furthermore, XPS showed that the resin engulfed the magnetite nanoparticles to a far greater extent. The difference in wetting behaviour of these coatings is largely attributed to their different morphologies, since the particles are similar sizes and TGA shows that the particles possess similar carboxylate grafting densities. The uneven distribution of nanoparticles in the magnetite/ epoxy resin coating is due to the particles' magnetic properties, which drive nanoparticle agglomeration as the coatings solidify. This work demonstrates that it is important to consider inter-particle interactions when fabricating low wettability composite coatings.

1. Introduction

Fabrication of robust, easy to apply, low wettability coatings still remains a major challenge within the research community. Thin films created using functionalized nanoparticles have been shown to possess rough surface textures that show superhydrophobic behaviour [1-5]. Deposition of the nanoparticles onto surfaces has been readily achieved through dipping [3,6] and spraying [2,5], which could make it suitable for use within a variety of different industrial and commercial sectors. For example, low wettability nanoparticle coatings could assist the removal of corrosive ions in aqueous solutions from metals, prevent cardboard getting wet during transport or storage, and facilitate the quick-drying of plastics. A large variety of nanoparticles have been shown to display this behaviour, such as metal oxides like ZnO [4] and Al_2O_3 [2,5], SiO_2 [1,3], and amorphous

carbon [7]. In these reports, the surface energy of metal oxide and SiO_2 nanoparticles is lowered through adsorption of suitable carboxylic acids [2,4,5] or alkylsilanes [1,3,8].

Despite their potential utility, these coatings possess relatively poor durability and can be easily removed through abrasion. Methods have been reported where nanoparticle adhesion has been improved through partial thermal embedding of the particles into materials such as glass [9] and graphene [10]. Alternatively, it has been shown that composite coatings can be prepared through embedding nanoparticles in materials such as silica [11] and polymers [7,12-14]. These coatings show greatly enhanced durability relative to films formed solely from the nanoparticles. For example, Manca *et al.* created a robust superhydrophobic coating through thermally embedding trimethylsiloxane functionalised SiO_2 nanoparticles into an organosilica matrix [11]. The organosilica binder was prepared using a sol-gel method and the resulting composite material was observed to maintain low wettability in outdoor exposure tests [11]. Similarly, Bayer *et al.* fabricated a robust water-repellent coating through annealing alternating layers of SiO_2 nanoparticles and fluoroalkyl methacrylic copolymer [13]. Coatings were prepared that remained superhydrophobic after pencil hardness, tape adhesion and linear abrasion tests [13].

Although these coatings showed good durability, many of these approaches require relatively high temperatures in order to thermally embed the particles in the matrix materials. Lower temperature routes for creating superhydrophobic nanoparticle/ composite coatings have been achieved using commercially available adhesives [16-19]. In these reports, superhydrophobic coatings were prepared at room temperature, or at temperatures of less than 80 °C. By comparison, embedding functionalised SiO_2 nanoparticles into organosilica was carried out at 350 °C [11]. In addition to their low temperatures, approaches utilising resin are also attractive since it has been shown that the resin and the nanoparticles can be combined and applied onto substrates in one step [17,19]. However, the proportions of the different materials need to be carefully controlled so that the resin does not engulf the particles. For example, Ebert and Bhushan demonstrated that highly durable, superhydrophobic coatings could be created using suspensions containing phosphonate functionalised nanoparticles and methylphenyl silicone resin [19]. It was observed that the coatings retained their superhydrophobic properties following water jet impact tests, indicating that they could function well as self-cleaning surfaces [19].

We have investigated whether this promising methodology can be used to improve the adhesion of isostearate functionalised Al_2O_3 and magnetite (Fe_3O_4) nanoparticles. Isostearic acid is a highly branched carboxylic acid that possesses alkyl moieties terminated

with several methyl groups [2]. Methyl groups have lower surface energy than methylene groups [2]. Consequently, this acid could be better suited for use in superhydrophobic coatings since the CH_3:CH_2 ratio per alkyl chain is larger than carboxylic acids with linear alkyl chains[2]. Previously, we have reported superhydrophobic coatings formed from isostearate functionalised Al_2O_3 nanoparticles [2]. However, to the best of our knowledge, the wetting properties of carboxylate functionalised magnetite nanoparticles have not previously been reported. Magnetite nanoparticles have been used to remove harmful metallic species from waste water [20-22] and Fe (II and III) compounds have been shown to immobilise bacteria and viruses [23-25]. Consequently, the use of magnetite nanoparticles in self-cleaning coatings would be desirable since they could remove pathogens and harmful materials from the environment.

2. Experimental methods

2.1. Materials and reagents

Al_2O_3 nanoparticles (d = 13 nm, 99.8%) and Fe_3O_4 nanoparticles (d = 15-20 nm, 99.5%) were purchased from Sigma-Aldrich and US Research Nanomaterials respectively. Isostearic acid was kindly provided by Nissan Chemical Industries and was used without further purification. Toluene and isopropanol were supplied by VWR Chemicals. SP106 Multi-Purpose Epoxy Resin System Slow Hardener was purchased from MB Fibreglass. Plastic film (75 micron thickness, 5-ply ethylene-vinyl acetate/ethylene-vinyl acetate/polyvinylidene chloride/ ethylene-vinyl acetate/ ethylene-vinyl acetate) was selected as the substrate in this study.

2.2. Synthesis of the isostearate functionalized metal oxide nanoparticles

The isostearate functionalized Al_2O_3 nanoparticles were synthesized using a method that we have previously reported [2]. Functionalisation of the isostearate functionalized magnetite nanoparticles was conducted through a similar method. In a typical experiment, magnetite nanoparticles (1.0 g, 4.3 mmol, 1.0 equiv.) were refluxed in toluene (100 mL) with isostearic acid (3.7 g, 12.9 mmol, 3.0 equiv.) for approximately twenty-four hours, under mechanical stirring. Once the reaction time had elapsed, the mixture was centrifuged at 5000 rpm for one hour to remove any physisorbed carboxylic acids from the nanoparticles. The supernatant was then removed and the resulting nanoparticulate slurry dried at 80 °C for at least three hours.

2.3. Preparation of the nanoparticle coatings

Various amounts of epoxy resin were added to isopropanolic suspensions containing Al_2O_3 and magnetite nanoparticles. The mass of the metal oxide nanoparticles in the suspensions was controlled so that 0.33 g of Al_2O_3 and Fe_3O_4 nanoparticles were added to the suspension per 20 mL of isopropanol. Three layers of nanoparticle/ epoxy resin (at various ratios) were spray coated onto the substrates to ensure full coverage of the surface by the films. Following this, the coated substrates were heated at 70 °C for three hours to accelerate the curing of the resin. Selected samples were then also sonicated in isopropanol for ten minutes, in order to remove particles that were less strongly embedded in the plastic. The mass ratios of the nanoparticles: epoxy resin in the functionalised Al_2O_3: resin coatings were 8.6:1.0, 2.0:1.0, 1.5:1.0, 1.0:1.0 and 1.0:1.5. The mass ratios of the nanoparticles: epoxy resin for the functionalised Fe_3O_4: resin coatings were 11.8:1.0, 6.5:1.0, 2.0:1.0, 1.0:1.0 and 1.0:1.5. In these experiments, the Fe_3O_4 nanoparticles were observed to be far more readily covered by the epoxy resin than the Al_2O_3 nanoparticles. Consequently, slightly different nanoparticle: resin ratios were selected for the two coatings in order to highlight the differences in agglomeration behaviour of the nanoparticles. As a comparison, coatings formed from pure isostearate functionalised Al_2O_3 and Fe_3O_4 nanoparticles (without resin) were spray coated onto the substrate from a 2% wt isopropanol suspension. Three layers of nanoparticles were deposited onto the substrate to ensure the surface was fully covered by the particles. Similarly to as with the nanoparticle/ resin coatings, some samples were then sonicated in isopropanol for ten minutes in order to remove particles from the samples. During the experiments, some measurements were performed on two or more samples from each type of nanoparticle / resin (1.0:1.0 ratio) coating as well as the coatings formed from the nanoparticles without resin. This was carried out to study whether there were any differences between the properties of the coatings on different samples. In each case the coatings showed similar properties (similar static water contact angles, surface morphologies etc.). The remaining experiments with various nanoparticles to resin ratios were performed on one set of samples.

2.4. Characterization

Water contact angle (WCA) measurements were obtained by the sessile drop method (resulting static contact angle, advanced and receding contact angle) using a DSA25 Expert Drop Shape Analyzer (Krüss), under ambient conditions using DI water. The Ellipse Tangent

1 method was used as the fitting method to measure the WCAs. Measurements were made using 4 μL droplets of deionised water under ambient conditions. The WCAs quoted in this study are the average of three measurements performed at different locations on the surfaces. For each surface, the uncertainty (±) that is associated with each WCA value is the difference between the average WCA and the measured WCA that was furthest away from the average. The measurements were not carried out as a function of time and were typically made after 20-30 s in order to maintain consistency between samples. Scanning electron microscopy (SEM) was performed on the Al_2O_3 and magnetite nanoparticle epoxy resin coatings using a Hitachi S4800 scanning electron microscope equipped with a Silicon Drift X-Max EDX detector. EDX spectra were analysed using Inca EDX software (Oxford Instr.). SEM was performed on the magnetite nanoparticle coating without epoxy resin using a JSM-7800F scanning electron microscope. X-ray photoelectron spectroscopy was performed using an Axis Supra XPS using a monochromated Al K_α source and large area slot mode detector (ca. 300 × 800 μm^2) analysis area. Spectra were recorded using a charge neutralizer to limit differential charging and binding energies were calibrated to the main hydrocarbon peak (BE 284.8 eV). The XPS data was analysed using CASA software with Shirley backgrounds. Infrared spectroscopy was performed using a Thermoscientific i510 instrument with attached ATR. Four scans were recorded during each measurement with a resolution of 4 cm^{-1}. Thermogravimetric analysis (TGA) was performed using TA Instrument SDT Q600 in an open alumina crucible under continuous air flow. During TGA, the magnetite particles were heated from ambient temperature to 800 °C at 20 °C.min^{-1}. BET was performed using a Quantachrome Nova 2000e instrument. Zeta potential measurements were performed using a Malvern Zetasizer nanoseries on suspensions containing 50 ppm isostearate functionalized Al_2O_3 and Fe_3O_4 nanoparticles in isopropanol. Atomic force microscopy (AFM) was carried out using a JPK Nanowizard AFM in tapping mode. Surface roughness values for the films were measured from 10.0 × 10 .0 μm^2 areas of the surfaces (Fig. S6).

3. Results and Discussion

3.1. Characterization of the isostearate functionalized magnetite nanoparticles

XPS and IR spectroscopy were carried out to investigate whether isostearic acid had adsorbed onto the surface of the magnetite nanoparticles. The characterisation of the isostearate functionalised Al_2O_3 nanoparticles has been reported previously [2]. In our previous study, IR spectroscopy showed that isostearic acid had chemisorbed onto the surface of the Al_2O_3 nanoparticles as a carboxylate. TGA showed that the chemisorbed isostearate on the Al_2O_3 had a grafting density of 2.0 nm^{-2}, whilst SEM showed that spray coating the functionalised particles onto surfaces generated densely packed nanoparticle films [2].

Consequently, it is not discussed here. The XPS spectrum of the as received Fe_3O_4 nanoparticles shows Fe and O photoelectron and auger electron peaks from the metal oxide (Fig. S1) [26]. A C 1s photoelectron peak is also observed in the spectrum, which is ascribed to the presence of some adventitious carbon, which could be oxygen containing hydrocarbon species (alcohols, ethers etc), or biological molecules [27]. Analysis of the elemental composition of the particles showed that it was composed of 45.7% O, 26.8% C, and 27.4% Fe.

The elemental composition of the functionalised magnetite nanoparticles was 36.6% O, 44.6% C, and 18.8% Fe. Since the amount of C is increased and the amount of Fe is reduced, relative to the as received magnetite, this suggests that isostearic acid adsorbs onto the surface of the nanoparticles. In line with this, the area of the C-O component of the O 1s peak is substantially greater than in the XPS spectrum of the as received nanoparticles (Fig. 1a and b). In the XPS spectra, the peak ascribed to the Fe-O component is observed at about 529.9 eV, whereas the peak ascribed to the C-O component is observed at approximately 531.2 eV [27,28]. Prior to functionalisation with isostearic acid, the ratio of the Fe-O: C-O peak area is approximately 2.3. This ratio changes to about 1.6 after refluxing the particles with isostearic acid, providing further evidence that the carboxylic acid had adsorbed onto the nanoparticles.

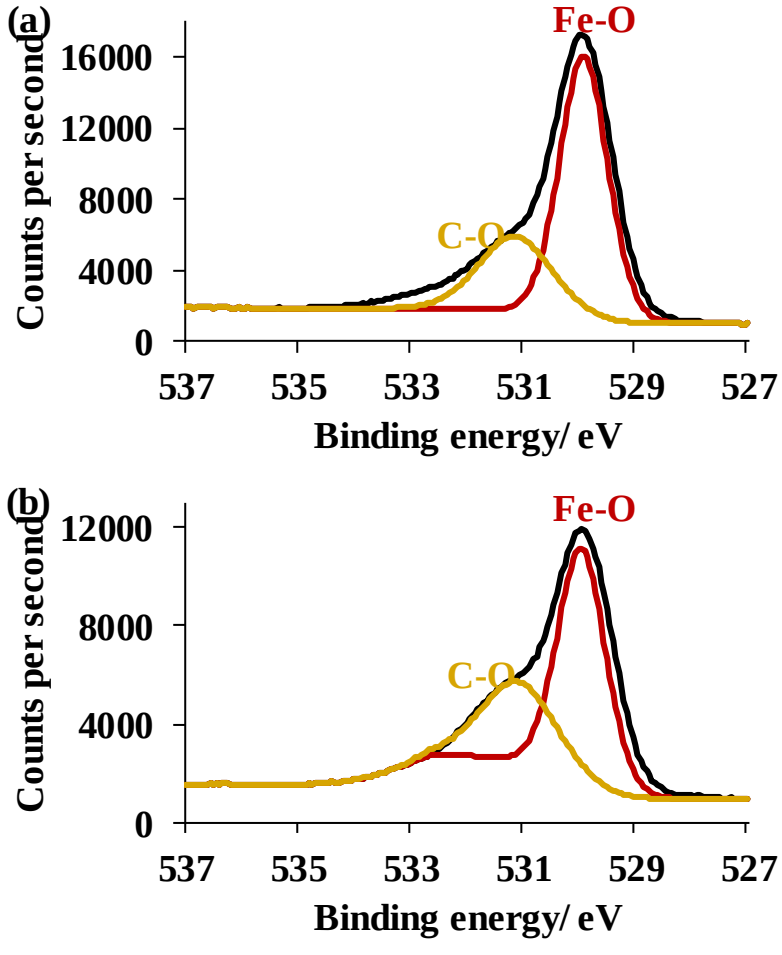

Fig. 1. High-resolution XPS data of the O 1s region of the as received magnetite nanoparticles (a), and the magnetite nanoparticles after refluxing with isostearic acid in toluene (b).

IR spectroscopy was used in order to examine the nature of the adsorbed carboxylic acid on the surface of the particles. The IR spectrum of the as received Fe_3O_4 nanoparticles (Fig. S2) shows a strong band ascribed to Fe-O stretching between 780-650 cm^{-1} [29]. In addition, O-H bending and stretching bands are observed at approximately 1630 cm^{-1} (Fig. 2a) and between 3570 and 3100 cm^{-1} respectively [30]. These bands are ascribed to the presence of hydroxyl groups that are present on the surface of the nanoparticles. Weak bands ascribed to C-H stretching of some adsorbed carbonaceous material are also observed between 2980-2850 cm^{-1} [31], as is shown in Fig S2 of the supporting materials.

Substantially more intense C-H stretching bands are observed in the IR spectrum of the functionalised nanoparticles (Fig. S3) [31]. In addition, bands ascribed to CH_2 scissoring and CH_3 umbrella modes from the alkyl chain of isostearic acid are also observed at about 1454 and 1377 cm^{-1} respectively [31, 32]. Unlike the IR spectrum of the as received isostearic acid (Figure 2b), a C=O stretching band is not observed in the IR spectrum of the functionalised nanoparticles (Figure 2c). This indicates that isostearic acid chemisorbs onto the surface of the particles as a carboxylate and no unreacted acid is left in the product [2,31]. In our previous publication we have reported the IR spectra of isostearate chemisorbed onto Al_2O_3 nanoparticles, which show carboxylate asymmetric stretching bands at about 1560 cm^{-1} [33]. A weak band at about 1515 cm^{-1} and a more intense band at approximately 1411 cm^{-1} (α) (Fig. 2c) are observed in the IR spectrum of isostearate functionalised Fe_3O_4 nanoparticles, which are not present in the IR spectra of the as received nanoparticles or the pure acid. We tentatively ascribe these bands to be due to carboxylate asymmetric and symmetric stretching of chemisorbed isostearate, in line with previously reported data [31, 34].

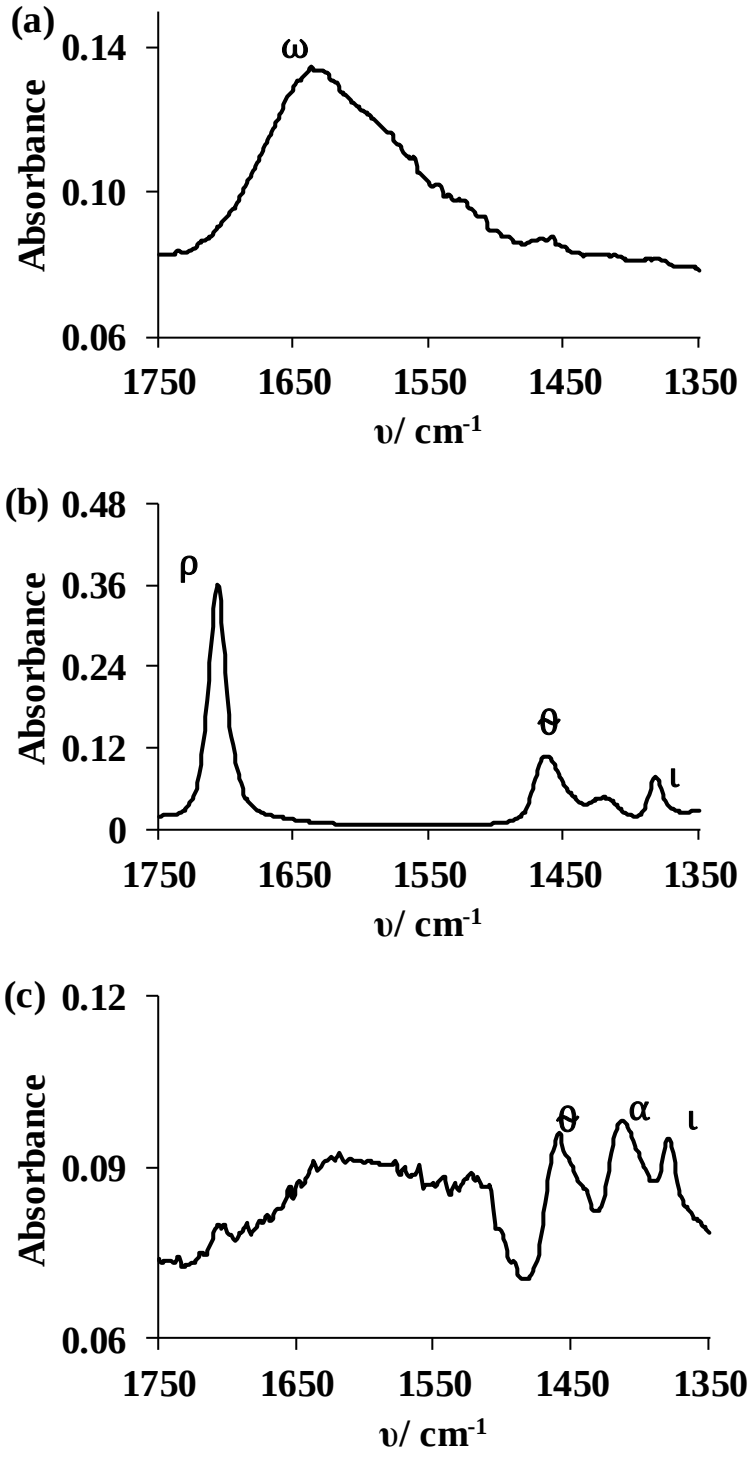

Fig. 2. FTIR spectra (1750-1350 cm^{-1}) of the as received magnetite nanoparticles (a), isostearic acid (b), and the magnetite nanoparticles after refluxing with isostearic acid in toluene (c). ω O-H, ρ C=O, θ CH_2, α CO_2^- (symmetric stretching), ι CH_3.

TGA was used to determine the grafting density of chemisorbed isostearate on the surface of the magnetite nanoparticles. The as-received magnetite nanoparticles were

observed to show a weight loss of approximately 4.28 % after heating to 800 °C (Fig. 3). The derivative of the TGA curve shows that the largest weight losses occur at about 95 and 200 °C. The former of these is ascribed to loss of water and volatile compounds, whilst the latter is due to desorption of the adventitious carbon that is observed using IR spectroscopy and XPS. TGA of the functionalized magnetite showed a weight loss of 9.45 % after heating to the same temperature (Fig. 3). The derivative of the TGA curve for the functionalised nanoparticles is largest at about 300 °C. The weight loss at this temperature is ascribed to desorption of chemisorbed isostearate from the surface of the nanoparticles. Assuming that the weight loss less than 100 °C is due to the removal of water and volatile compounds, and taking the surface area of the as received material to be 75.7 m^2g^{-1} (BET), the grafting density [5] of isostearic acid can be calculated to be 2.7 nm^{-2}. This value is in line with our previous functionalization of alumina nanoparticles with isostearic acid.

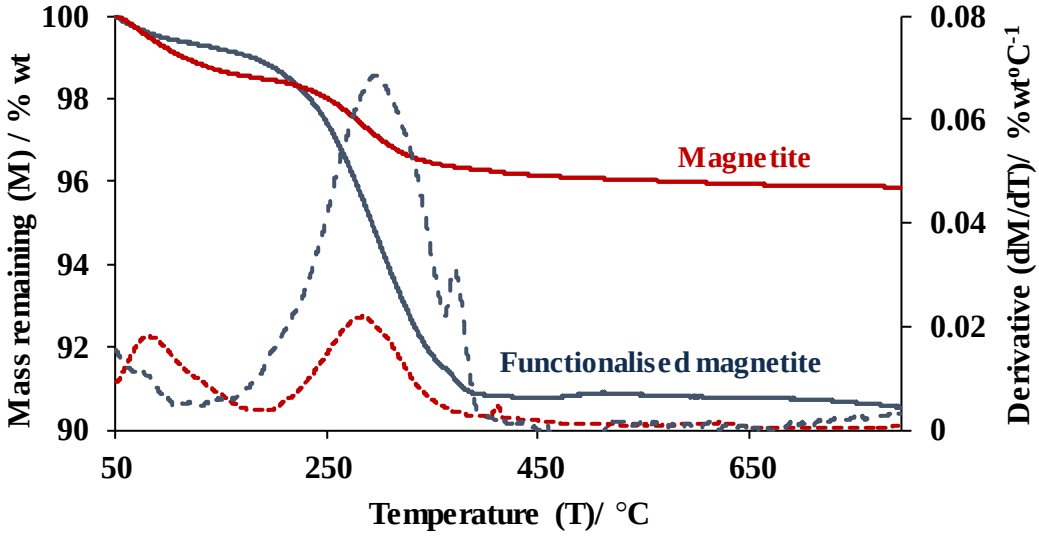

Fig 3. TGA data of the magnetite particulates, dashed curves correspond to derivatives.

Coatings formed from isostearate functionalised magnetite were observed to be superhydrophobic. For example, the WCA of the nanoparticles on the plastic substrate was observed to be approximately 151.9 ± 2.0° (Fig. 4, inset). By comparison, the WCA of a coating of the as received nanoparticles was observed to be 107.2 ± 3.6°, confirming that the low wettability of the coating is due to the presence of the adsorbed carboxylates. The as received Al_2O_3 nanoparticle coating was more hydrophilic compared to the magnetite nanoparticle coating and displayed a WCA of 56.3 ± 8.7° when spray coated onto the plastic. Interestingly, SEM showed that discrete areas of the substrate were not covered by the

nanoparticles (Fig. 4), despite the surface showing superhydrophobic behaviour. Typically, the agglomerates that were observed were less than 10 μm in size.

It has been discussed in related reports that the dispersibility of nanoparticles in liquids is related to the relative magnitudes of the magnetic and van der Waals forces between the particles, in addition to the electrostatic forces that the particles experience [34]. The former of these two forces are attractive and drive nanoparticle agglomeration, whereas the latter is repulsive and promotes the formation of stable dispersions [35]. Zeta potential measurements were employed to study the agglomeration behaviour of the functionalized nanoparticles in isopropanol. It was observed that the zeta potential of both of the functionalised Al_2O_3 and magnetite nanoparticles in isopropanol was similar (ca. 35-45mV), suggesting that the increased agglomeration behaviour of the magnetite nanoparticles was not due to weaker electrostatic forces [36]. Since both of these types particles also have similar diameters, it is plausible that the increased agglomeration of the magnetite nanoparticles could be due to their magnetic properties.

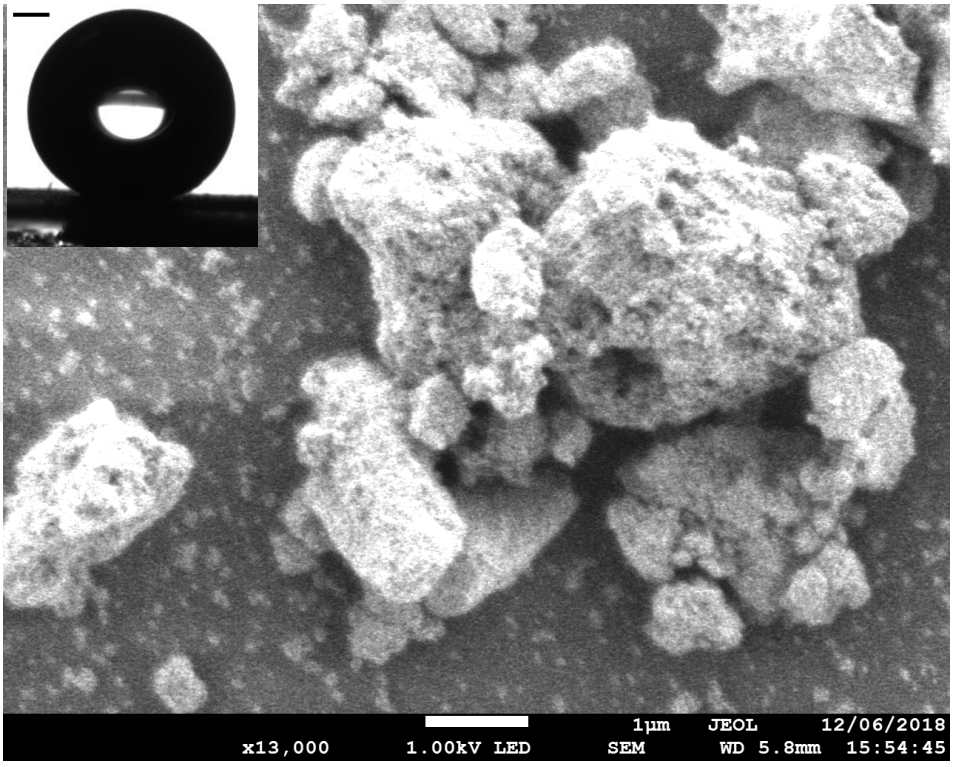

Fig. 4. SEM image of the isostearate functionalised magnetite nanoparticles spray coated onto the plastic substrate. An image of a water droplet on the surface is shown in the inset (scale bar = 0.5 mm).

3.2. Characterization of the nanoparticle/ epoxy resin coatings

WCA measurements were performed on the nanoparticle/ epoxy resin coatings to study how the incorporation of resin into the coatings affects their wettability as well as durability. In order to establish the optimum nanoparticle/resin ratio at which the highest contact angle was achieved, various nanoparticle/resin ratios were mixed and tested. Prior to the addition of epoxy resin, coatings formed from the isostearate functionalised Al_2O_3 nanoparticles were observed to be superhydrophobic and displayed WCAs of about 151.1 ± 1.0°. Coatings were prepared where the mass ratio of the nanoparticles: epoxy resin was varied between 8.6:1.0 and 1.0:1.4 (Fig. 5). It was observed that coatings prepared using mass ratios between 2.0:1.0 and 1.0:1.0 displayed WCAs between 149-150°. Increasing the mass ratio further created less hydrophobic surfaces with WCAs below 140°, suggesting that the resin was engulfing the nanoparticles to a larger extent. The WCA of a coating solely formed from the resin was measured to be 100.8 ± 1.5°, which confirmed that the nanoparticles were largely responsible for increasing the hydrophobicity of the plastic.

Following sonication in isopropanol, the WCAs of the coatings were reduced by about 8-15°, indicating that there were loose particles present that were not embedded in the resin. By comparison, sonication in isopropanol was observed to remove at least the majority of the nanoparticles from the substrate when resin was not incorporated into the coatings. Substrates showed WCAs approximately equal to that of the plastic film (ca. 86°) after sonication, indicating that epoxy resin substantially improves nanoparticle adhesion onto the substrate.

Incorporation of epoxy resin into coatings formed from the functionalised magnetite nanoparticles was observed to create much more hydrophilic surfaces. Large increases in surface wettability occurred even when a relatively small amount of epoxy resin was added to the nanoparticle suspensions. For example, a coating formed from an 11.8:1.0 mass ratio of nanoparticles to epoxy resin displayed a WCA of 124.3 ± 10.6° (Fig. 6). Increasing the amount of epoxy resin in the suspensions was found to increase the hydrophilicity of the surfaces further. Coatings with mass ratios between 6.5:1.0 and 1.0:1.5 were prepared and it

was observed that the WCAs progressively reduced until they reached values between 75-80° (Fig. 6), similar to that of coatings formed solely of the epoxy resin.

These results indicate that the resin covers the magnetite nanoparticles to a much greater extent, relative to when the Al_2O_3 nanoparticles are used in the coatings. In addition to being less hydrophobic, the nanoparticles on the surface, which affect the WCA, are also easier to remove through sonication. This was evidenced from the drop in WCA when 11.8:1.0 ratio coating was sonicated in isopropanol, as is shown in Fig. 6.

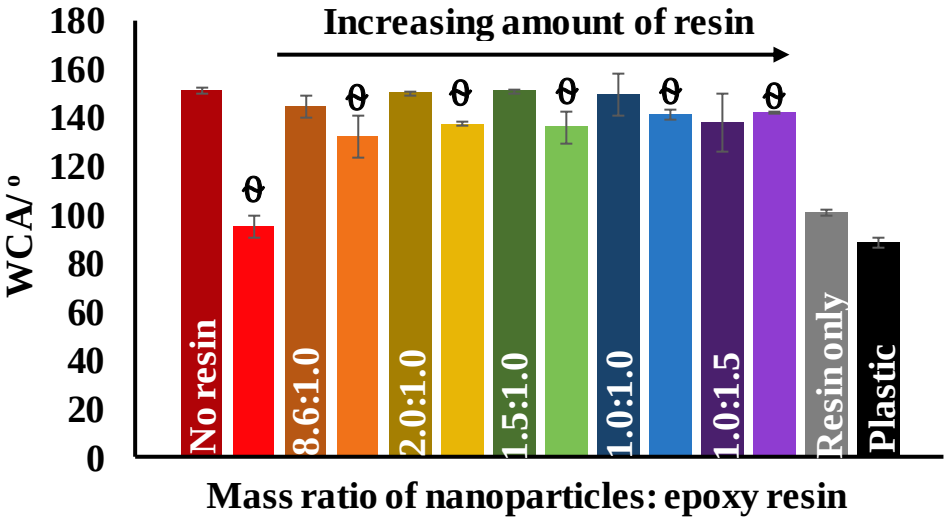

Fig. 5. Average WCA values of the Al_2O_3 nanoparticle/ epoxy resin coatings. θ series show the WCAs of the coatings after sonication in isopropanol for ten minutes.

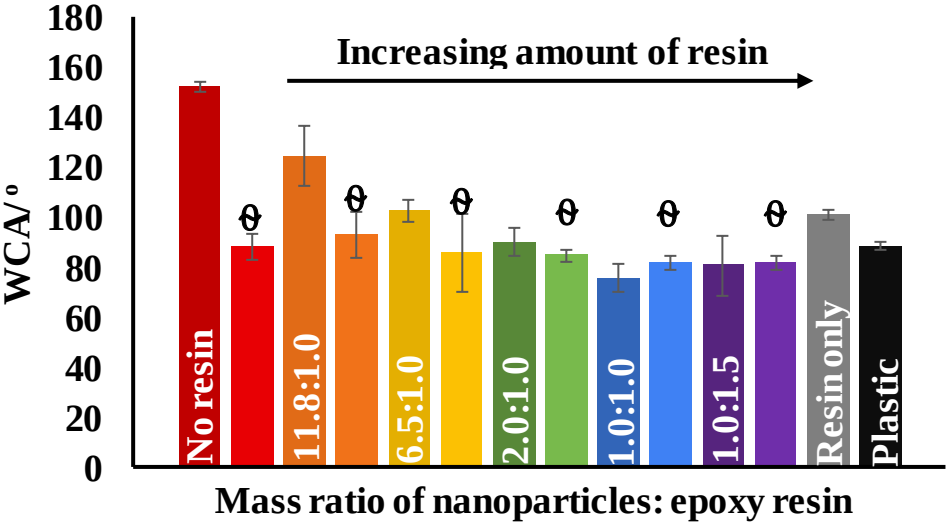

Fig. 6. Average WCA values of the magnetite nanoparticle/ epoxy resin coatings. θ series show the WCAs of the coatings after sonication in isopropanol for ten minutes.

SEM and XPS were used to study the morphology and elemental composition of coatings prepared using equal masses of nanoparticles and epoxy resin. As can be seen in Figure 7a, the morphology of the coating containing the Al_2O_3 nanoparticles was relatively homogenous, indicating the particles were evenly distributed amongst the resin. However, the morphology of the coating formed from the magnetite nanoparticles showed discrete areas where agglomerates of particles were present (Fig. 7b). EDX showed that the areas surrounding the particles were largely comprised of epoxy resin (Fig. S4). Peaks assigned to Cu and Br were observed in the EDX spectra of this surface. However, they were also observed in the EDX spectrum of the as received plastic substrate (Fig. S5), indicating that their origin was not ascribed to material in the coating. Similarly to films formed solely from the magnetite nanoparticles, this behaviour is ascribed to the particles' magnetic properties. Attractions between the nanoparticles could lead to agglomeration of the nanoparticles as the epoxy resin cures, thus explaining the morphological differences that are observed using SEM.

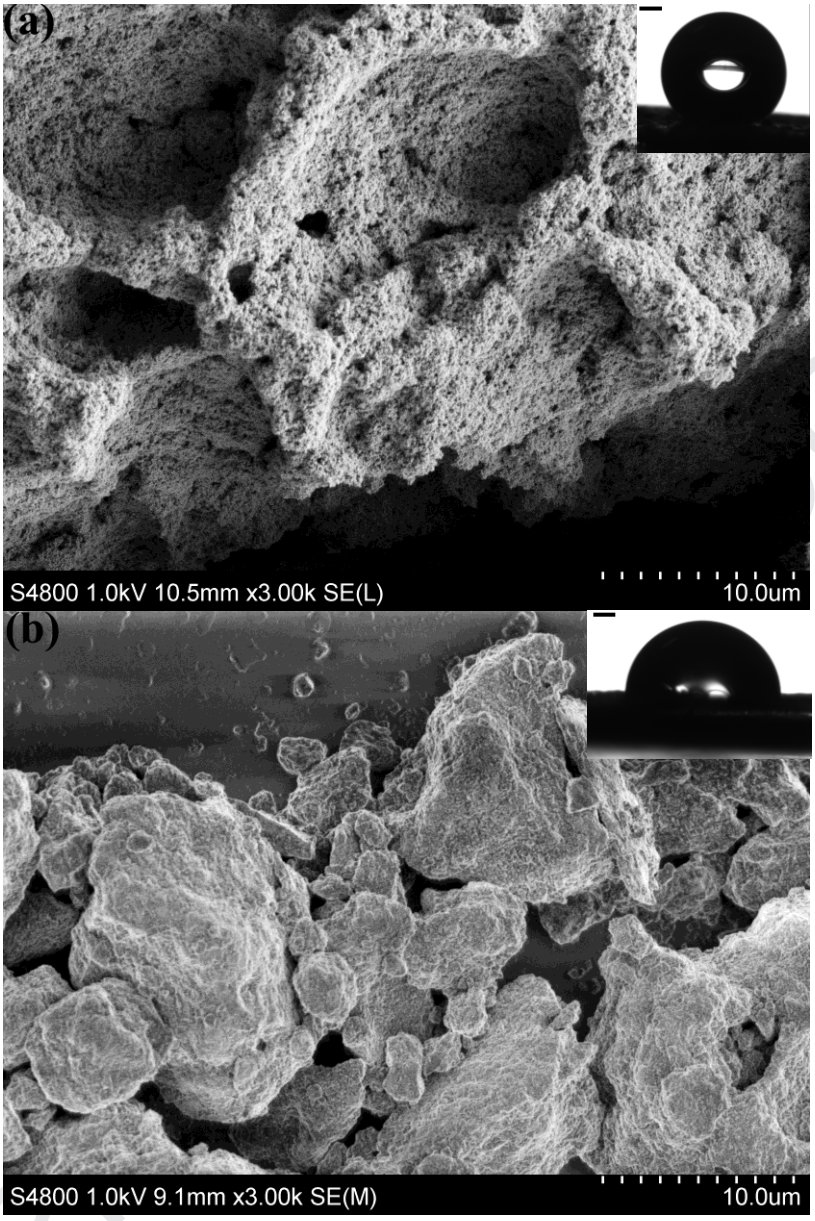

Fig. 7. SEM images of the nanoparticle coatings containing equal masses of nanoparticles and epoxy resin. (a) the morphology of the Al_2O_3 coating and (b) the morphology of the Fe_3O_4 coating. Images of H_2O droplets on the surfaces are shown in the insets (scale bars = 0.5 mm).

XPS showed that the elemental composition of the Al_2O_3 coating was 29.9 ±0.9 % O, 53.3 ±2 .2% C, 1.1 ± 0.0% N, and 16.4 ± 0.5% Al. A survey spectrum of this coating is displayed in Fig. 8a. The presence of N can be explained since amines are present in the resin to affect cross-linking [37]. The atomic percentages of these elements were not observed to change by more than about 1%, following sonication of the coating in isopropanol. This

indicates that the uppermost surface layers remain largely comprised of Al_2O_3 nanoparticles, in line with the highly hydrophobic WCA of this coating.

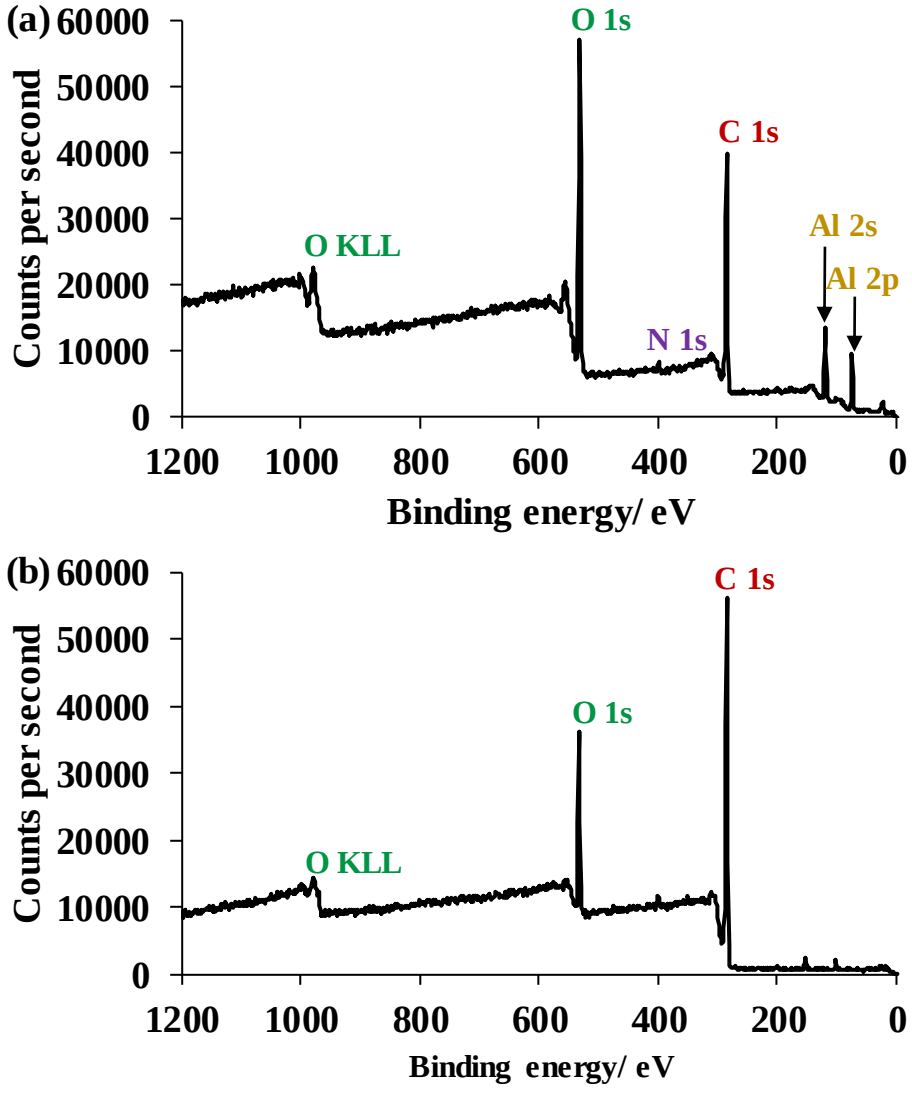

Fig. 8. XPS survey spectra of the nanoparticle coatings containing equal masses of nanoparticles and epoxy resin: (a) the spectrum of the Al_2O_3 coating, (b) the spectrum of the magnetite coating.

By comparison, Fe photoelectron peaks were not detected when XPS was performed on the coating containing the magnetite nanoparticles (Fig. 8b and Fig. 9a), indicating that they had been completely covered by the epoxy resin. Photoelectron peaks ascribed to Fe were observed in the coating prepared using a suspension containing a mass ratio of 11.8:1.0 magnetite nanoparticles: epoxy resin (Fig. 9b). However, the atomic percentages of this

surface were observed to be 15.5 ±0.5% O, 82.8 ±0.1% C, and 1.7 ±1.0% Fe, indicating that only small amounts of resin are required to cover the nanoparticles.

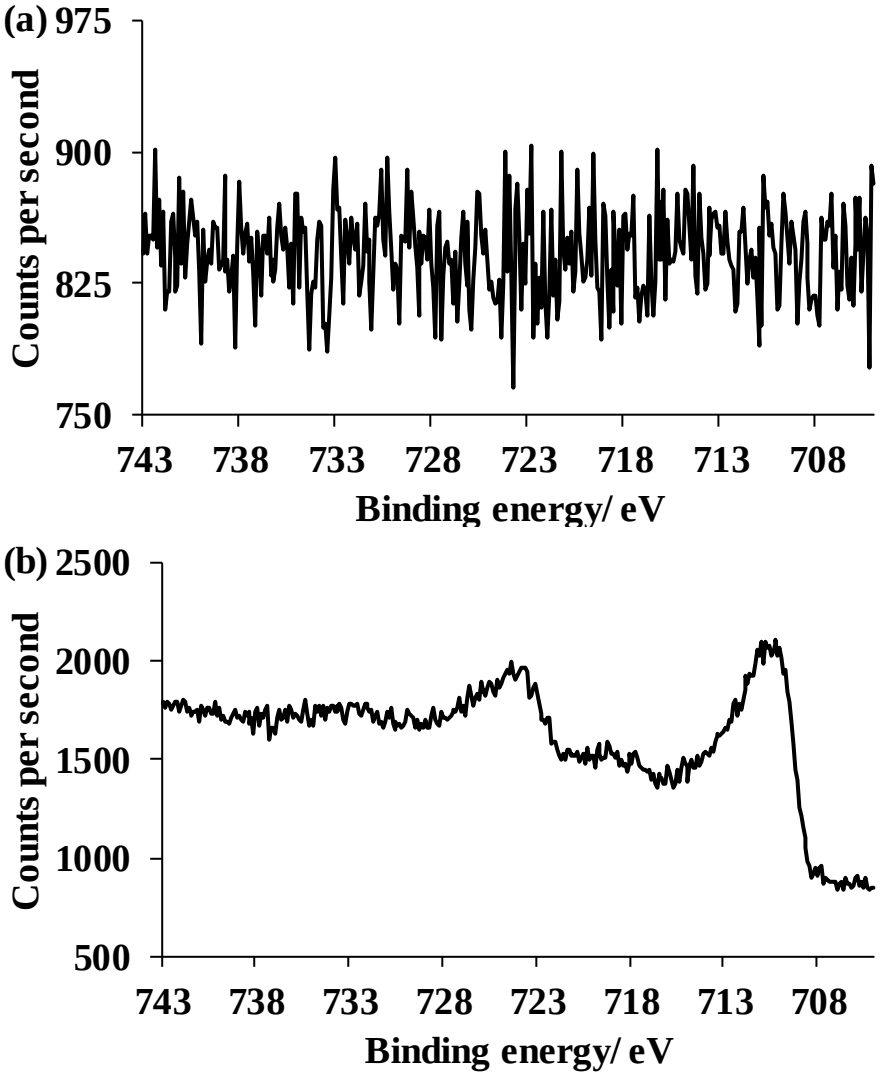

Fig. 9. High resolution XPS data of (a) the Fe 2p region of a magnetite coating containing equal masses of nanoparticles and epoxy resin, and (b) the Fe 2p region of a magnetite coating created using a 11.8:1.0 mass ratio of nanoparticles to epoxy resin.

AFM was used to study the surface roughness of the nanoparticle coatings. It was observed that both of the functionalised nanoparticle coatings showed substantially larger topographies than the as received plastic, and displayed similar surface roughness (Table 1). Incorporation of epoxy resin into the spray coating suspensions was observed to generate coatings with even greater topographies. However, the 1.0:1.0 functionalised nanoparticles:

epoxy resin coatings possessed similar surface roughness parameters, despite the substantial differences in the WCA values. These results show that the arrangement of nanoparticles in the surface layers plays a role in influencing the wettability of the surface, in addition to surface topography.

Table 1. Surface roughness parameters of the plastic and the nanoparticle coatings. Values were calculated from 10.0 × 10.0 μm2 AFM images (SI fig. 6)

Surface	Average roughness (R_a) (nm)	Root mean squared roughness (R_q) (nm)	Peak to valley roughness (R_t) (nm)
Plastic	19	24	156
Functionalized Al_2O_3 nanoparticles	155	210	2067
Functionalized Fe_3O_4 nanoparticles	151	226	1829
1.0:1.0 functionalized Al_2O_3 nanoparticles: epoxy resin	276	344	2131
1.0:1.0 functionalized Fe_3O_4 nanoparticles: epoxy resin	272	374	2041

Dynamic WCA measurements were also performed on the nanoparticle coatings to study the adhesion of H_2O droplets onto the surfaces. It was observed that the hysteresis of the nanoparticle coatings increased when resin was incorporated in the coatings, indicating that the water droplets became more adherent when the surface contained epoxy resin (Table 2). However, the hysteresis increase observed when resin was added to the Al_2O_3 coating was only approximately 6 °, indicating that water was only slightly more adherent onto the surface relative to when the coating solely containing the nanoparticles. By comparison, the hysteresis angle from the functionalised Fe_3O_4 nanoparticles and the resin was substantially larger than the plastic (Table 2), which shows that it could not function as a water repellent surface.

Table 2. Dynamic WCA values of the plastic and the nanoparticle coatings.

Surface	Advancing WCA (°)	Receding WCA (°)	Hysteresis (°)
Plastic	109.5 ± 0.5	83.7 ± 1.5	25.8
Functionalized Al_2O_3 nanoparticles	159.9 ± 3.9	146.8 ± 5.4	13.1
Functionalized Fe_3O_4 nanoparticles	161.6 ± 3.4	150.9 ± 9.1	10.7
1.0:1.0 functionalized Al_2O_3 nanoparticles: epoxy resin	151.0 ± 4.2	131.8 ± 9.0	19.2
1.0:1.0 functionalized Fe_3O_4 nanoparticles: epoxy resin	110.5 ± 4.8	33.5 ± 3.8	77

The durability of the Al_2O_3 coating was further investigated through subjecting the coated substrate to ethanol washing and tissue-wipe tests. Ethanol washing was not observed to significantly affect the wettability of the substrate. WCAs of about 147° were observed after washing (Fig. S7a). Tissue-wiping was observed to remove loose and weakly embedded particles from the coating causing it to become slightly less hydrophobic. However, despite this, the surface was still highly hydrophobic and displayed a WCA of about 140° (Fig. S7b). This indicates that enough particles remain embedded in the coating for it to show low wetting behaviour.

4. Conclusions

Durability and wetting behaviour of coatings formed from carboxylate functionalized Al_2O_3 and Fe_3O_4 nanoparticles and epoxy resin was thoroughly studied and compared using SEM, Contact angle, XPS and AFM measurements. Although previous works [16-19] have shown that commercially available adhesives can improve the wear resistance of hydrophobic nanoparticle coatings, none of these approaches have studied the affect of changes in surface morphology and chemistry on the wettability of these composite systems. Surface geometry has a large bearing on wetting and water-repellent properties of a surface [1, 38]. Consequently, it is pertinent to study in depth how additives that are incorporated into coatings to improve their durability interact with the material that is added to make the surface hydrophobic, and how this interaction changes the surface geometry.

Highly hydrophobic coatings that displayed WCAs between 145-150° were prepared using green hydrocarbon functionalized Al_2O_3 nanoparticles and epoxy resin. These coatings showed good durability when subjected to sonication in organic solvents and tissue-wipe tests. By comparison, combining functionalized magnetite nanoparticles of similar size with epoxy resin created coatings that were far less hydrophobic and displayed WCAs between about 75-125°. SEM showed that the nanoparticles in the magnetite/epoxy resin coating were present as large agglomerates, whereas the Al_2O_3 nanoparticles were more evenly distributed across the surface of the coating. XPS also showed that the epoxy resin engulfs the magnetite nanoparticles to a far greater extent. Consequently, the difference in wettability of these two coatings can be explained on this basis. The increased agglomeration of the magnetite nanoparticles is largely due to their magnetic properties, since both types of particle are similar in size and show similar carboxylate grafting densities.

This work advances the research into the development of durable hydrophobic coatings since it shows that nanoparticle agglomeration has a significant bearing of wettability when the particles are combined with commercially available adhesives. Furthermore, it shows that magnetic nanoparticles are less suitable for incorporation into hydrophobic coatings containing epoxy resin on the grounds of increased agglomeration behaviour, relative to non-magnetic particles. This is important since magnetic nanoparticles, such as iron oxides, can also be used to remove harmful metals from water [20-22], and have been observed to immobilise bacteria and viruses [23-25]. Consequently, their employment in hydrophobic coatings could be useful. This research is important because it shows that it is necessary to investigate methods for creating durable hydrophobic coatings using Fe_3O_4 nanoparticles that do not involve adhesives such as epoxy resin. Further work from our group is underway to investigate how the durability of hydrophobic nanoparticle films can be improved through embedding the particles into plastics. This approach would eliminate the need for durability enhancement using adhesives, thereby circumventing the problem of nanoparticle agglomeration in discrete areas of the adhesive.

Acknowledgment

Financial support was provided by the Welsh Government Sêr Cymru Programme through Sêr Cymru II Welsh Fellowship part funded by the European Regional Development Fund (ERDF) (S.A.) and the Sêr Cymru Chair for Low Carbon Energy and Environment (A.R.B.). The Robert A. Welch Foundation (C-0002) is acknowledged for additional support (A.R.B.). Salts Healthcare Ltd. is also thanked for financial support (D.H). We would like to

acknowledge the assistance provided by Swansea University College of Engineering AIM Facility, which was funded in part by the EPSRC (EP/M028267/1), the European Regional Development Fund through the Welsh Government (80708) and the Sêr Solar project via Welsh Government. We would also like to acknowledge Dr Daniel Jones and Dr Athanasios Koutsianos from Swansea University for their help with the XPS and BET measurements.

Appendix A. Supplementary material

Supplementary data associated with this article can be found, in the online version. XPS and IR spectra of the as received magnetite nanoparticles. SEM images and EDX spectra of the as received plastic substrate. AFM images of the as received plastic and functionalized nanoparticles with and without resin. Images of water droplet on the Al_2O_3 nanoparticles/epoxy resin after washing with ethanol and wiping with tissue.

References

[1] T.J. Athauda, D.S. Decker, R.R. Ozer, Effect of surface metrology on the wettability of SiO_2 nanoparticle coating, Mater. Lett., 67 (2012) 338-341.

[2] S. Alexander, J. Eastoe, A.M. Lord, F. Guittard, A.R. Barron, Branched hydrocarbon low surface energy materials for superhydrophobic nanoparticle derived surfaces, ACS Appl. Mater. Interfaces, 8 (2016) 660-666.

[3] R.G. Karunakaran, C.-H. Lu, Z. Zhang, S. Yang, Highly transparent superhydrophobic surfaces from the coassembly of nanoparticles (<100 nm), Langmuir, 27 (2011) 4594-4602.

[4] N. Agrawal, S. Munjal, M.Z. Ansari, N. Khare, Superhydrophobic palmitic acid modified ZnO nanoparticles, Ceram. Int., 43 (2017) 14271-14276.

[5] W.A.- Shatty, A.M. Lord, S. Alexander, A.R. Barron, Tunable surface properties of aluminum oxide nanoparticles from highly hydrophobic to highly hydrophilic, ACS Omega, 2 (2017) 2507-2514.

[6] Z. Cui, L. Yin, Q. Wang, J. Ding, Q. Chen, A facile dip-coating process for preparing highly durable superhydrophobic surface with multi-scale structures on paint films, J. Colloid Interface Sci., 337 (2009) 531–537.

[7] I.S. Bayer, A.J. Davis, A. Biswas, Robust superhydrophobic surfaces from small diffusion flame treatment of hydrophobic polymers, RSC Adv., 4 (2014) 264-268.

[8] Z.-T. Li, B. Lin, L.-W. Jiang, E.-C. Lin, J. Chen, S.-J. Zhang, Y.-W. Tang, F.-A. He, D.-H. Li, Effective preparation of magnetic superhydrophobic Fe_3O_4/PU sponge for oil-water separation, Appl. Surf. Sci., 427 (2018) 56–64.

[9] T. Karakouz, B.M. Maoz, G. Lando, A. Vaskevich, I. Rubinstein, Stabilization of gold nanoparticle films on glass by thermal embedding, ACS Appl. Mater. Interfaces, 3 (2011) 978-987.

[10] Q. Xi, X. Chen, D.G. Evans, W. Yang, Gold nanoparticle-embedded porous graphene thin films fabricated via layer-by-layer self-assembly and subsequent thermal annealing for electrochemical sensing, Langmuir, 28 (2012) 9885-9892.

[11] M. Manca, A. Cannavale, L. De Marco, A.S. Arico, R. Cingolani, G. Gigli, Durable superhydrophobic and antireflective surfaces by trimethylsilanized silica nanoparticles-based sol-gel processing, Langmuir, 25 (2009) 6357-6362.

[12] L. Cao, A.K. Jones, V.K. Sikka, J. Wu, D. Gao, Anti-icing superhydrophobic coatings, Langmuir, 25 (2009) 12444-12448.

[13] I.S. Bayer, K.G. Krishnan, R. Robison, E. Loth, D.H. Berry, T. E. Farrell, J.D. Crouch, Thermal alternating polymer nanocomposite (TAPNC) coating designed to prevent aerodynamic insect fouling, Sci. Rep., 6 (2016) 38459.

[14] I.S. Bayer, A.J. Davis, E. Loth, A. Steele, Water jet resistant superhydrophobic carbonaceous films by flame synthesis and tribocharging, Mater. Today Commun., 3 (2015) 57-68.

[15] S. Naderizadeh, A. Athanassiou, I.S. Bayer, Interfacing superhydrophobic silica nanoparticle films with graphene and thermoplastic polyurethane for wear/abrasion resistance, J. Colloid Interface Sci., 519 (2018) 285-295.

[16] B. Chen, J. Qiu, E. Sakai, N. Kanazawa, R. Liang, H. Feng, Robust and superhydrophobic surface modification by a “paint + adhesive” method: applications in self-cleaning after oil contamination and oil–water separation, ACS Appl. Mater. Interfaces, 8 (2016) 17659-17667.

[17] Y. Si, F. Yang, Z. Guo, Bio-inspired one-pot route to prepare robust and repairable micro-nanoscale superhydrophobic coatings, J. Colloid Interface Sci., 498 (2017) 182–193.

[18] Y. Lu, S. Sathasivam, J. Song, C.R. Crick, C.J. Carmalt, I.P. Parkin, Robust self-cleaning surfaces that function when exposed to either air or oil, Science, 347 (2015) 1132-1135.

[19] D. Ebert, B. Bhushan, Transparent, superhydrophobic, and wear-resistant coatings on glass and polymer substrates using SiO_2, ZnO, and ITO nanoparticles, Langmuir, 28 (2012) 11391-11399.

[20] J. Liu, Z. Zhao, G. Jiang, Coating Fe_3O_4 magnetic nanoparticles with humic acid for high efficient removal of heavy metals in water, Environ. Sci. Technol., 42 (2008) 6949-6954.

[21] W. Yantasee, C.L. Warner, T. Sangvanich, R.S. Addleman, T.G. Carter, R.J. Wiacek, G.E. Fryxell, C. Timchalk, M.G. Warner, Removal of heavy metals from aqueous systems with thiol functionalized superparamagnetic nanoparticles, Environ. Sci. Technol., 41 (2007) 5114-5119.

[22] Y.-C. Chang, D.-H. Chen, Preparation and adsorption properties of monodisperse chitosan-bound Fe_3O_4 magnetic nanoparticles for removal of Cu(II) ions, J. Colloid Interface Sci., 283 (2005) 446-451.

[23] S.J. Maguire-Boyle, M.V. Liga, Q. Li, A.R. Barron, Alumoxane/ferroxane nanoparticles for the removal of viral pathogens: the importance of surface functionality to nanoparticle activity, Nanoscale, 4 (2012) 5627-5632.

[24] L.A. Warren, F.G. Ferris, Continuum between sorption and precipitation of Fe(III) on microbial surfaces, Environ. Sci. Technol., 32 (1998) 2331-2337.

[25] X. Châtellier, D. Fortin, M. M. West, G. G. Leppard، F. G. Ferris, Effect of the presence of bacterial surfaces during the synthesis of Fe oxides by oxidation of ferrous ions, Eur. J. Mineral., 13 (2001) 705-714.

[26] J.F. Moulder, W.F. Stickle, P.E. Sobol, K.D. Bomben in Handbook of X-ray Photoelectron Spectroscopy, Perkin-Elmer Corporation, 1992, Appendix H, pp. 256.

[27] J. Landoulsi, M.J. Genet, S. Fleith, Y. Touré, I. Liascukiene, C. Méthivier, P.G. Rouxhet, Organic adlayer on inorganic materials: XPS analysis selectivity to cope with adventitious contamination, Appl. Surface Sci., 383 (2016) 71-83.

[28] J. Yang, P. Zou, L. Yang, J. Cao, Y. Sun, D. Han, S. Yang, Z. Wang, G. Chen, B. Wang, X. Kong, A comprehensive study on the synthesis and paramagnetic properties of PEG-coated Fe_3O_4 nanoparticles, Appl. Surface Sci., 303 (2014) 425-432.

[29] Y.F. Shen, J. Tang, Z.H. Nie, Y. D. Wang, Y. Ren, L. Zuo, Preparation and application of magnetic Fe_3O_4 nanoparticles for wastewater purification, Sep Purif Technol., 68 (2009) 312-319.

[30] A. Putnis in an Introduction to mineral sciences, Cambridge University Press, 1992, Ch.4, pp. 95.

[31] R.R. Sahoo, S.K. Biswas, Frictional response of fatty acids on steel, J. Colloid Interface Sci., 333 (2009) 707-718.

[32] L. Senak, M.A. Davies, R. Mendelsohn, A quantitative ir study of hydrocarbon chain conformation in alkanes and phospholipids: CH_2 wagging modes in disordered bilayer and H_{II} phases, J. Phys. Chem., 95 (1991) 2565-257.

[33] D. Hill, H. Attia, A.R. Barron, S. Alexander, Size and morphology dependent surface wetting based on hydrocarbon functionalized nanoparticles, J. Colloid Interface Sci., 543 (2019) 328-334.

[34] G. Kataby, M. Cojocaru, R. Prozorov, A. Gedanken, Coating carboxylic acids on amorphous iron nanoparticles, Langmuir, 15 (1999) 1703-1708.

[35] H. Yan, J. Zhang, C. You, Z. Song, B. Yu, Y. Shen, Influences of different synthesis conditions on properties of Fe_3O_4 nanoparticles, Mater. Chem. Phys., 113 (2009) 46-52.

[36] R.R. Retamal Marín, F. Babick, L. Hillemann, Zeta potential measurements for non-spherical colloidal particles – practical issues of characterisation of interfacial properties of nanoparticles, Colloids Surf. A, 532 (2017) 516-521.

[37] K. Dušek in Rubber-Modified Thermoset Resins, American Chemical Society, 1984, Ch.1, pp. 3-14.

[38] M. Miwa, A. Nakajima, A. Fujishima, K. Hashimoto, T. Watanabe, Effects of the Surface Roughness on Sliding Angles of Water Droplets on Superhydrophobic Surfaces, Langmuir 16 (2000) 5754-5760.